

Journal Pre-proofs

Research paper

Novel ferrocene-based 1,2,3-triazolyl compounds: Synthesis, anti-migration properties and catalytic effects on oxidizers during combustion

Wenqian Cheng, Xiaoling Shi, Yu Zhang, Yajun Jian, Guofang Zhang

PII: S0020-1693(19)31769-4
DOI: <https://doi.org/10.1016/j.ica.2019.119374>
Reference: ICA 119374

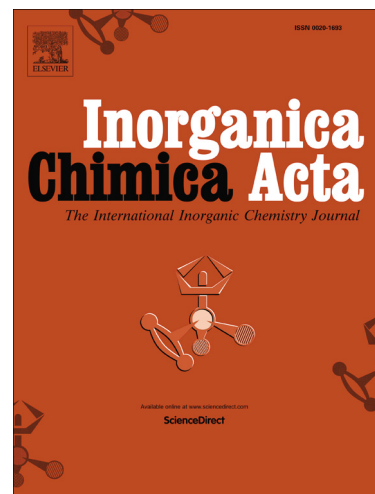
To appear in: *Inorganica Chimica Acta*

Received Date: 14 November 2019
Revised Date: 15 December 2019
Accepted Date: 15 December 2019

Please cite this article as: W. Cheng, X. Shi, Y. Zhang, Y. Jian, G. Zhang, Novel ferrocene-based 1,2,3-triazolyl compounds: Synthesis, anti-migration properties and catalytic effects on oxidizers during combustion, *Inorganica Chimica Acta* (2019), doi: <https://doi.org/10.1016/j.ica.2019.119374>

This is a PDF file of an article that has undergone enhancements after acceptance, such as the addition of a cover page and metadata, and formatting for readability, but it is not yet the definitive version of record. This version will undergo additional copyediting, typesetting and review before it is published in its final form, but we are providing this version to give early visibility of the article. Please note that, during the production process, errors may be discovered which could affect the content, and all legal disclaimers that apply to the journal pertain.

© 2019 Published by Elsevier B.V.



Novel ferrocene-based 1,2,3-triazolyl compounds: Synthesis, anti-migration properties and catalytic effects on oxidizers during combustion

Wenqian Cheng, Xiaoling Shi, Yu Zhang, Yajun Jian and Guofang Zhang*

Key Laboratory of Applied Surface and Colloid Chemistry, School of Chemistry and Chemical Engineering, Shaanxi Normal University, Xi'an, 710119, China

Abstract: To tackle high-migratory and high-volatility problem of marketed neutral ferrocene-based burning rate catalysts, twenty-one ferrocene-based 1,2,3-triazolyl compounds (**Fc-TAZs**) were synthesized by click reaction and characterized completely by NMR, FT-IR, UV-Vis and elemental analysis. In addition, four compounds were structurally confirmed by single crystal X-ray diffraction. TG and DSC analysis showed that the new **Fc-TAZs** are of high thermal stability. Cyclic voltammetry investigations suggested that more than half of the **Fc-TAZs** are reversible redox systems. Anti-migration and anti-volatility tests revealed that all the **Fc-TAZs** display, on comparison with Catocene, extremely low volatility and migration tendency due to the appearance of polar oxygen and nitrogen atoms in their molecules. Catalytic activity tests of the novel **Fc-TAZs** towards the thermal decomposition of oxidizers, evaluated by TG and DSC techniques, indicated that all **Fc-TAZs** exert great effects on the thermal disintegration of AP and compounds **5**, **7** and **11** can promote the thermal decomposition of HMX during combustion.

Keywords: ferrocene-based 1,2,3-triazolyl compounds; click reaction; thermal stability; anti-migration property; combustion catalysis

1. Introduction

Composite solid propellants are heterogeneous propellants consisting mainly of oxidizers and polymeric binders (metal powder is also usually added). In an aluminized ammonium perchlorate (AP)-based solid propellant a ferrocene derivative is commonly added to enhance burning rate and

*Corresponding authors. G. F. Zhang: Tel:+86-29-81530830; Fax: +86-29-81530727; E-mail address: gfzhang@snnu.edu.cn

decrease pressure exponent of the propellant [1-4].

Although the commercialized ferrocene-based burning rate catalysts (BRCs), such as tert-butylferrocene (TBF), n-butylferrocene (NBF) and 2,2-Bis(ethylferrocenyl)propane (Catocene), have shown highly catalytic efficiency in the composite solid propellants, they bear some unavoidable problems due to their lower molecular weights and neutral nature. They could sublime during fabrication of the propellants and move gradually to the surface and interface of the propellant columns after long-time storage [3,4]. This type of high-migratory deficiency can lead to non-uniform distribution of BRCs in the propellants. During combustion process of the propellants this defect will enlarge burning area and increase pressure in the chamber of the rocket engine due to rapid decomposition of the migrated BRCs, and finally increase explosion danger of the propellants. Therefore, in order to extend service life of the propellants and decrease military expenses, it is necessary to develop low and even non-migratory ferrocene derivatives as BRCs.

In recent decades great efforts have been devoted to design and synthesize ferrocene derivatives as BRC candidates with low migration tendency and high catalytic activity. A few effective methods have been adopted to deal with the issues of the neutral BRCs, for examples, increasing molecular weight or molecular polarity of the small neutral ferrocene derivatives, grafting ferrocenyl groups on the polymer or dendrimer chains, introducing concepts of ionic liquid and coordination compound into ferrocene derivatives [5-26]. D. Saranvannakumar, T. Jana, et al developed low- and even non-migratory ferrocenyl-functionalized polymers or dendrimers [5-9]. H. Y. Zhao, Y. F. Yuan and our group prepared a large number of metal complexes derived from ferrocenyl ligands [15-20]. C. Morales-Verdejo and coworkers evaluated anti-migratory ability and combustion catalytic performance of some homo- and hetero-nuclear conjugated metallocenes with Fe (II), Co (II), Ni(II) or Mn (II) as central metals and found that all metallocenes show low migration trends and high combustion catalytic performance in the thermal decomposition of AP [11,12]. L. Wang group used ferrocenecarbonyl chloride as a precursor and synthesized a series of ferrocenyl esters, amides and hydroquinones by condensation reactions [21,22]. Our group designed and synthesized hundreds of energetic ionic ferrocenyl compounds to enhance anti-migration ability and catalytic activity of the neutral BRCs [23-26]. Although hundreds of novel ferrocene derivatives have been reported to tackle the high-migration issues and

enhance catalytic activity of the neutral ferrocene-based BRCs, the existing problems have not been well solved yet.

Copper-catalyzed azide alkyne cycloaddition (CuAAC), also known as "click reaction", has been developed for many years [27-29]. Ferrocene-based 1,2,3-triazolyl compounds have been reported mainly as ionic recognition sensors, antifungal and anticancer medicines, etc. [30-33]. Their application in composite solid propellants as BRCs is limited, however [34]. Herein, based on straightforward construction and nitrogen-rich feature of 1,2,3-triazolyl groups, we have designed and synthesized a series of ferrocenyl 1,2,3-triazolyl compounds (**Fc-TAZs**) (Scheme 1) by CuAAC method to enhance anti-migratory property and to ameliorate catalytic activity of the marketed ferrocene-based BRCs in composite solid propellants. The molecular structures of the novel **Fc-TAZs** were characterized completely by ^1H NMR, ^{13}C NMR, FT-IR, UV-Vis spectroscopies, elemental analysis and some of them additionally by single-crystal X-ray diffraction. Their thermal stability were investigated by TG and DSC. Electrochemical properties were measured by cyclic voltammetry (CV). Anti-migration and anti-volatility performances were determined with Catocene and ferrocene (Fc) as references. Their catalytic activities towards the thermal degradation of AP, RDX and HMX were measured by DSC and TG techniques.

(Please insert Scheme 1 here)

2. Experimental

2.1. Materials and equipment

Hydroxymethylferrocene was purchased from Xuzhou Guanrong Pharmaceutical & Chemical Co., Ltd, China. AP, RDX and HMX were gained from Xi'an Modern Chemistry Research Institute. Azidomethylferrocene was prepared according to the synthetic procedure as described [35]. ^1H and ^{13}C NMR spectra were performed on a Bruker Avance 400 MHz spectrometer. UV-Vis absorption spectra were recorded on a UV-2450 spectrophotometer. Elemental analyses were conducted with a Vario EL III Elemental Analyzer. DSC and TG studies were achieved on HS-1 and Q50 models, respectively, under nitrogen atmosphere (50 mL min^{-1}) at $5^\circ\text{C}\cdot\text{min}^{-1}$ with sample mass around 3.0 mg. Cyclic voltammetry (CV) studies were executed on a CHI660C analyzer with a platinum electrode for working and an Ag/Ag^+ electrode as the

reference. In the CV determination experiments the compounds were solved in 0.1 mol L⁻¹ n-Bu₄PF₆-DMSO supporting electrolyte.

2.2. Synthesis

Since the synthetic procedures of the new **Fc-TAZs 1–21** are identical, 1-ferrocenylmethyl-1*H*-1,2,3-triazol-4-yl-methyl phenyl ether (**1**) was taken as an example [36,37]: To a 20 mL DMF solution of phenol 1.14 g (15.0 mmol), 5.18 g (37.5 mmol) K₂CO₃ was added and stirred at 60 °C for 1 h and then 1.42 ml (18.1 mmol) propargyl bromide was added dropwise and the reaction mixture was kept stirring and heating at 60 °C for 8 h until completion of the reaction, the reaction mixture was then cooled to room temperature and filtered. The filtrate was evaporated to dryness. The crude 2-propargyl phenyl ether was purified by column chromatography using petroleum ether/ethyl acetate (v:v) 5:1 as eluent to collect the purified intermediate 2-propargyl phenyl ether. To a 100 mL round-bottom flask containing 0.41 g (3.12 mmol) 2-propargyl phenyl ether and 0.75 g (3.12 mmol) azidomethylferrocene in 30 ml methanol was added a solution of 0.23 g (0.94 mmol) CuSO₄ 5H₂O in 15 ml water. A freshly prepared solution of 0.19 g (0.94 mmol) sodium ascorbate in 15 ml water was added and the reaction solution was stirred at room temperature for 24 h. After the solvents were removed under vacuum, the residue was eluted from a chromatographic column using dichloromethane/methanol (v:v) 50:1. The solvents were evaporated to dryness and the residue was dried to collect the desired product **1**.

1-Ferrocenylmethyl-1*H*-1,2,3-triazol-4-ylmethyl phenyl ether (1). Yellow powder. Yield: 1.024 g (88%). M. p.: 110 °C (DSC). FT-IR (KBr): $\nu = 3434$ m, 3087 m, 2894 w, 2859 w, 1598 s, 1494 s, 1452 w, 1314 w, 1251 vs, 1168 m, 1050 s, 1002 w, 822 s, 760 s, 691 m, 490 m cm⁻¹. ¹H NMR (400 MHz, DMSO-d₆): δ 8.20 (s, 1H), 7.28 (t, $J = 7.6$ Hz, 2H), 7.01 (d, $J = 8.4$ Hz, 2H), 6.94 (t, $J = 7.6$ Hz, 1H), 5.32 (s, 2H), 5.10 (s, 2H), 4.34 (s, 2H), 4.19 (s, 7H). ¹³C NMR (101 MHz, DMSO-d₆): δ 159.65 (OC), 145.53 (NCCH), 130.95 (NCCH), 123.45, 122.64, 116.19 (C₆H₅), 82.13, 70.53, 70.36 (C₅H₄), 70.35 (C₅H₅), 63.45 (C₅H₄CH₂), 51.57 (OCH₂). Calcd. C₂₀H₁₉FeN₃O(373.09): C, 64.36; H, 5.13; N, 11.26 %; Anal. Found: C, 64.30; H, 5.19; N, 11.23%.

Bis(ferrocenylmethyl-1*H*-1,2,3-triazol-4-ylmethyl) hydroquinone ether (2). Yellow powder. Yield: 1.751 g (84%). M. p.: 207.3 °C (DSC). FT-IR (KBr): $\nu = 3441$ m, 3149 w, 3073 w,

2921 w, 2866 w, 1626 m, 1501 vs, 1460 m, 1335 m, 1231 vs, 1106 m, 1037 s, 815 s, 732 w, 503 m cm^{-1} . $^1\text{H NMR}$ (400 MHz, DMSO-d_6): δ 8.16 (s, 2H), 6.93 (s, 4H), 5.31 (s, 4H), 5.03 (s, 4H), 4.34 (s, 4H), 4.18 (s, 14H). $^{13}\text{C NMR}$ (101 MHz, DMSO-d_6) δ 153.67 (OC), 145.08 (NCCH), 122.89 (NCCH), 116.73 (C_6H_4), 81.59, 70.01, 69.84 (C_5H_4), 69.82 (C_5H_5), 63.62 ($\text{C}_5\text{H}_4\text{CH}_2$), 51.03 (OCH₂). Calcd. $\text{C}_{34}\text{H}_{32}\text{Fe}_2\text{N}_6\text{O}_2$ (668.13): C, 61.10; H, 4.83; N, 12.57 %; Anal. Found: C, 61.02; H, 4.88; N, 12.52%.

Bis(ferrocenylmethyl-1*H*-1,2,3-triazol-4-ylmethyl) resorcinol ether (3). Yellow powder. Yield: 1.688 g (81%). M. p.: 150.1 °C (DSC). FT-IR (KBr): ν = 3441 m, 3087 w, 2935 w, 2866 w, 1591 vs, 1487 m, 1460 m, 1383 m, 1341 m, 1279 s, 1182 vs, 1147 vs, 1106 m, 1009 s, 815 s, 725 m, 490 s cm^{-1} . $^1\text{H NMR}$ (400 MHz, DMSO-d_6): δ 8.19 (s, 2H), 7.16 (t, J = 8.0 Hz, 1H), 6.68 (s, 1H), 6.60 (d, J = 6.0 Hz, 2H), 5.32 (s, 4H), 5.07 (s, 4H), 4.34 (s, 4H), 4.19 (s, 14H). $^{13}\text{C NMR}$ (101 MHz, CDCl_3): δ 160.86 (OC), 145.31 (NCCH), 131.46 (NCCH), 123.52, 109.00, 103.55 (C_6H_4), 82.13, 70.54, 70.38 (C_5H_4), 70.35 (C_5H_5), 63.53 ($\text{C}_5\text{H}_4\text{CH}_2$), 51.56 (OCH₂). Calcd. $\text{C}_{34}\text{H}_{32}\text{Fe}_2\text{N}_6\text{O}_2$ (668.13): C, 61.10; H, 4.83; N, 12.57 %; Anal. Found: C, 61.01; H, 4.90; N, 12.51%.

Bis(ferrocenylmethyl-1*H*-1,2,3-triazol-4-ylmethyl) catechol ether (4). Yellow powder. Yield: 1.918 g (92%). M. p.: 153.2 °C (DSC). FT-IR (KBr): ν = 3441 m, 3087 w, 2935 w, 2866 w, 1591 vs, 1487 m, 1460 m, 1383 m, 1341 m, 1279 s, 1182 vs, 1147 vs, 1106 m, 1009 s, 815 s, 725 m, 490 s cm^{-1} . $^1\text{H NMR}$ (400 MHz, CDCl_3): δ 7.55 (s, 2H), 7.02 (m, 2H), 6.90 (m, 2H), 5.25 (s, 4H), 5.19 (s, 4H), 4.25 (t, J = 1.6 Hz, 4H), 4.19 (t, J = 1.6 Hz, 4H), 4.16 (s, 10H). $^{13}\text{C NMR}$ (101 MHz, CDCl_3): δ 148.44 (OC), 144.11 (NCCH), 122.51 (NCCH), 122.13, 115.47 (C_6H_4), 80.98, 69.02 (C_5H_4), 68.90 (C_5H_5), 63.55 ($\text{C}_5\text{H}_4\text{CH}_2$), 50.04 (OCH₂). Calcd. $\text{C}_{34}\text{H}_{32}\text{Fe}_2\text{N}_6\text{O}_2$ (668.13): C, 61.10; H, 4.83; N, 12.57 %. Anal. Found: C, 61.00; H, 4.89; N, 12.52 %.

O,O',O''-Tris(ferrocenylmethyl-1*H*-1,2,3-triazol-4-ylmethyl) phloroglucinol ether (5). Yellow powder. Yield: 2.404 g (80%). M. p.: 298.2 °C (dec, DSC). FT-IR (KBr): ν = 3441 m, 3094 w, 2928 w, 1591 vs, 1452 m, 1328 w, 1217 w, 1147 vs, 1113 m, 1044 vs, 1002 m, 822 s, 718 w, 490 s cm^{-1} . $^1\text{H NMR}$ (400 MHz, CDCl_3): δ 7.50 (s, 3H), 6.21 (s, 3H), 5.29 (s, 6H), 5.06 (s, 6H), 4.27 (s, 6H), 4.21 (s, 6H), 4.17 (s, 15H). $^{13}\text{C NMR}$ (101 MHz, CDCl_3): δ 160.95 (OC), 144.56 (NCCH), 123.08 (NCCH), 95.96 (C_6H_3), 81.61, 70.02, 69.86 (C_5H_4), 69.82 (C_5H_5), 63.00

(C₅H₄C_H₂), 51.03 (OCH₂). Calcd. C₄₈H₄₅Fe₃N₉O₃ (963.17): C, 59.84; H, 4.71; N, 13.08 %. Anal. Found: C, 59.68; H, 4.79; N, 13.02 %.

O,O',O''-Tris(ferrocenylmethyl-1*H*-1,2,3-triazol-4-ylmethyl) pyrogallol ether (6).

Yellow powder. Yield: 2.284 g (76%). M. p.: 198.2 °C (DSC). FT-IR (KBr): ν = 3441 w, 3094 w, 2921 w, 2353 w, 1591 s, 1473 s, 1300 m, 1244 s, 1091 vs, 1037 vs, 1002 s, 815 s, 732 w, 490 s cm⁻¹. ¹H NMR (400 MHz, CDCl₃): δ 7.65-7.55 (d, 3H), 6.89 (t, 1H), 6.63 (d, 2H), 5.24 (s, 4H), 5.19 (s, 2H), 5.10 (s, 6H), 4.27 (s, 4H), 4.20 (s, 2H), 4.18-4.10 (d, 21H). ¹³C NMR (101 MHz, CDCl₃): δ 153.28 (OC), 145.49, 144.86 (NCCH), 138.46 (OC), 124.99, 124.02 (NCCH), 123.49, 108.94 (C₆H₃), 82.22, 81.96, 69.92, 69.85 (C₅H₄), 69.79 (C₅H₅), 67.57, 64.15 (C₅H₄C_H₂), 50.98, 50.78 (OCH₂). Calcd. C₄₈H₄₅Fe₃N₉O₃ (963.17): C, 59.84; H, 4.71; N, 13.08 %. Anal. Found: C, 59.72; H, 4.82; N, 13.12 %.

Ferrocenylmethyl-1*H*-1,2,3-triazol-4-ylmethyl *p*-tert-butylphenol ether (7). Yellow powder. Yield: 1.218 g (91%). M. p.: 120.3 °C (DSC). FT-IR (KBr): ν = 3434 w, 3087 w, 2963 m, 2866 w, 1605 m, 1508 s, 1460 m, 1397 w, 1300 w, 1244 vs, 1182 s, 1106 m, 1044 s, 822 s, 753 w, 490 s cm⁻¹. ¹H NMR (400 MHz, CDCl₃): δ 7.51 (s, 1H), 7.30 (d, *J* = 8.4 Hz, 2H), 6.90 (d, *J* = 8.4 Hz, 2H), 5.29 (s, 2H), 5.15 (s, 2H), 4.42–3.98 (m, 9H), 1.28 (s, 9H). ¹³C NMR (101 MHz, CDCl₃): δ 156.89 (OC), 145.22 (NCCH), 144.80 (NCCH), 127.20, 122.91, 115.14 (C₆H₄), 81.67, 69.90 (C₅H₄), 69.82 (C₅H₅), 63.12 (C₅H₄C_H₂), 51.11 (OCH₂), 34.99 (CCH₃), 32.41 (CH₃). Calcd. C₂₄H₂₇FeN₃O₃ (429.15): C, 67.14; H, 6.34; N, 9.79 %. Anal. Found: C, 67.10; H, 6.38; N, 9.78 %.

Ferrocenylmethyl-1*H*-1,2,3-triazol-4-ylmethyl 2-nitrophenol ether (8) Yellow powder. Yield: 1.030 g (79%). M. p.: 107.5 °C (DSC). FT-IR (KBr): ν = 3427 w, 3087 w, 2921 m, 2866 w, 1612 m, 1522 vs, 1452 m, 1356 s, 1287 vs, 1251 m, 1050 s, 995 m, 822 s, 746 s, 691 w, 497 s cm⁻¹. ¹H NMR (400 MHz, CDCl₃): δ 7.83 (d, *J* = 15.2 Hz, 1H), 7.64 (s, 1H), 7.53 (t, *J* = 7.6 Hz, 1H), 7.31 (d, *J* = 8.4 Hz, 1H), 7.05 (t, *J* = 7.6 Hz, 1H), 5.34 (s, 2H), 5.30 (s, 2H), 4.28 (s, 2H), 4.22 (s, 2H), 4.17 (s, 5H). ¹³C NMR (101 MHz, CDCl₃): δ 151.56 (OC), 143.07 (NCCH), 140.10 (NO₂C), 134.31 (NCCH), 125.69, 122.59, 121.03, 115.44 (C₆H₄), 80.74, 69.13 (C₅H₄), 68.90 (C₅H₅), 63.79 (C₅H₄C_H₂), 50.23 (OCH₂). Calcd. C₂₀H₁₈FeN₄O₃ (418.07): C, 57.44; H, 4.34; N, 13.40 %. Anal. Found: C, 57.38; H, 4.30; N, 13.42 %.

Ferrocenylmethyl-1*H*-1,2,3-triazol-4-ylmethyl 4-nitrophenol ether (9) Yellow powder. Yield: 1.017 g (78%). M. p.: 153.8 °C (DSC). FT-IR (KBr): $\nu = 3434$ w, 3101 w, 2942 m, 2838 w, 1598 s 1508 vs, 1425 m, 1390 m, 1335 vs, 1265 s, 1113 s, 1009 m, 849 s, 801 s, 746 m, 691 w, 497 m cm^{-1} . **^1H NMR** (400 MHz, CDCl_3): δ 8.19 (d, $J = 8.8$ Hz, 2H), 7.53 (s, 1H), 7.06 (d, $J = 8.8$ Hz, 2H), 5.32 (s, 2H), 5.25 (s, 2H), 4.28 (s, 2H), 4.23 (s, 2H), 4.19 (s, 5H). **^{13}C NMR** (101 MHz, CDCl_3): δ 163.14 (OC), 142.54 (NCCH), 141.82 (NO_2C), 125.92 (NCCH), 122.41, 114.86 (C_6H_4), 80.36, 69.23, 69.00 (C_5H_4), 68.97 (C_5H_5), 62.46 ($\text{C}_5\text{H}_4\text{CH}_2$), 50.29 (OCH_2). Calcd. $\text{C}_{20}\text{H}_{18}\text{FeN}_4\text{O}_3$ (418.07): C, 57.44; H, 4.34; N, 13.40 %. Anal. Found: C, 57.38; H, 4.31; N, 13.43 %.

Bis(ferrocenylmethyl-1*H*-1,2,3-triazol-4-ylmethyl) 4,6-dinitrocatechol ether (10). Light brown powder. Yield: 2.105 g (89%). M. p.: 192.8 °C (dec, DSC). FT-IR (KBr): $\nu = 3419$ w, 3094 w, 2935 w, 1605 vs, 1522 s, 1404 m, 1341 m, 1293 s, 1224 m, 1030 m, 815 s, 746 w, 490 s cm^{-1} . **^1H NMR** (400 MHz, CDCl_3): δ 8.68 (s, 1H), 7.70 (s, 2 H), 7.64 (s, 1H), 5.46 (s, 4H), 5.31 (s, 4H), 4.29 (s, 4H), 4.23 (s, 4H), 4.19 (s, 10H). **^{13}C NMR** (101 MHz, CDCl_3): δ 156.80 (OC), 141.56 (NCCH), 131.47, 125.57 (NO_2C), 123.30 (NCCH), 101.98 (C_6H_2), 80.37, 69.25, 68.97 (C_5H_4), 68.94 (C_5H_5), 64.13 ($\text{C}_5\text{H}_4\text{CH}_2$), 50.36 (OCH_2). Calcd. $\text{C}_{34}\text{H}_{30}\text{Fe}_2\text{N}_8\text{O}_6$ (758.10): C, 53.85; H, 3.99; N, 14.78 %. Anal. Found: C, 53.80; H, 3.95; N, 14.81 %.

1-Ferrocenylmethyl-1*H*-1,2,3-triazol-4-ylmethyl benzoate (11) Yellow powder. Yield: 1.026 g (82%). M. p.: 153.7 °C (DSC). FT-IR (KBr): $\nu = 3108$ m, 2955 w, 1709 vs, 1605 m, 1438 m, 1328 m, 1265 vs, 1099 s, 1037 m, 815 m, 704 m, 497 s cm^{-1} . **^1H NMR** (400 MHz, CDCl_3): δ 8.02 (d, $J = 7.5$ Hz, 2H), 7.59 (s, 1H), 7.54 (d, $J = 14.8$ Hz, 1H), 7.41 (d, $J = 15.4$ Hz, 2H), 5.43 (s, 2H), 5.29 (s, 2H), 4.28 (d, $J = 3.4$ Hz, 2H), 4.22 (d, $J = 3.4$ Hz, 2H), 4.17 (s, 5H). **^{13}C NMR** (101 MHz, CDCl_3): δ 166.46 (OOC), 142.78 (NCCH), 133.17 (NCCH), 129.75, 128.37, 123.29 (C_6H_5), 80.65 (C_5H_5), 69.13, 68.98, 68.91 (C_5H_4), 58.11 ($\text{C}_5\text{H}_4\text{CH}_2$), 50.14 (OCH_2). Calcd. $\text{C}_{21}\text{H}_{19}\text{FeN}_3\text{O}_2$ (401.08): C, 62.86; H, 4.77; N, 10.47 %. Anal. Found: C, 62.74; H, 4.80; N, 10.42 %.

1-Ferrocenylmethyl-1*H*-1,2,3-triazol-4-ylmethyl *p*-nitrobenzoate (12) Light brown powder. Yield: 1.197 g (86%). M. p.: 145.6 °C (DSC). FT-IR (KBr): $\nu = 3094$ m, 2963 w, 1723 vs, 1605 m, 1529 s, 1348 m, 1265 vs, 1099 s, 1044 m, 815 m, 718 s, 497 s cm^{-1} . **^1H NMR** (400 MHz, CDCl_3): δ 8.26 (d, $J = 8.8$ Hz, 2H), 8.19 (d, $J = 8.8$ Hz, 2H), 7.60 (s, 1H), 5.46 (s, 2H), 5.31 (s, 2H), 4.30 (s, 2H), 4.23 (s, 2H), 4.18 (s, 5H). **^{13}C NMR** (101 MHz, CDCl_3): δ 165.45 (OOC),

151.52 (CNO₂), 142.85 (NCCH), 136.04 (NCCH), 131.79, 124.43, 124.32 (C₆H₄), 81.38, 70.09, 69.91 (C₅H₄), 69.84 (C₅H₅), 59.68 (C₅H₄CH₂), 51.12 (OCH₂). Calcd. C₂₁H₁₈FeN₄O₄ (446.07): C, 56.52; H, 4.07; N, 12.56 %. Anal. Found: C, 56.57; H, 4.00; N, 12.64 %.

1-Ferrocenylmethyl-1*H*-1,2,3-triazol-4-ylmethyl *o*-nitrobenzoate (13) Orange yellow powder. Yield: 1.072 g (77%). M. p.: 222.6 °C (dec, DSC). FT-IR (KBr): $\nu = 3094$ m, 2942 w, 1730 vs, 1605 m, 1529 vs, 1348 s, 1272 vs, 1127 s, 1050 s, 926 m, 829 s, 725 s, 490 s cm⁻¹. **¹H NMR** (400 MHz, CDCl₃): δ 7.90 (d, $J = 7.9$ Hz, 1H), 7.72 (d, $J = 7.2$ Hz, 1H), 7.64 (m, 3H), 5.45 (s, 2H), 5.31 (s, 2H), 4.30 (s, 2H), 4.23 (s, 2H), 4.18 (s, 5H). **¹³C NMR** (101 MHz, CDCl₃): δ 165.17 (OOC), 148.12 (CNO₂), 141.74 (NCCH), 132.99 (NCCH), 131.92, 129.97, 127.19, 123.94, 123.43 (C₆H₄), 80.70, 69.12 (C₅H₄), 68.92 (C₅H₅), 59.58 (C₅H₄CH₂), 50.19 (OCH₂). Calcd. C₂₁H₁₈FeN₄O₄ (446.07): C, 56.52; H, 4.07; N, 12.56 %; Anal. Found: C, 56.47; H, 4.03; N, 12.55%.

1-Ferrocenylmethyl-1*H*-1,2,3-triazol-4-ylmethyl 3,5-dinitrobenzoate (14) Dark brown powder. Yield: 1.088 g (71%). M. p.: 196.6 °C (DSC). FT-IR (KBr): $\nu = 3115$ m, 2921 w, 1730 vs, 1626 m, 1557 vs, 1348 vs, 1272 vs, 1162 s, 1044 m, 954 m, 822 m, 711 m, 490 m cm⁻¹. **¹H NMR** (400 MHz, DMSO-*d*₆): δ 9.03 (d, $J = 2.0$ Hz, 1H), 8.86 (s, 2H), 8.30 (s, 1H), 5.51 (s, 2H), 5.34 (s, 2H), 4.36 (s, 2H), 4.19 (s, 7H). **¹³C NMR** (101 MHz, DMSO-*d*₆): δ 163.65 (OOC), 149.78 (CNO₂), 142.38 (NCCH), 133.61 (NCCH), 130.24, 126.21, 124.02 (C₆H₃), 83.65, 70.11, 70.00 (C₅H₄), 69.76 (C₅H₅), 60.67 (C₅H₄CH₂), 50.35 (OCH₂). Calcd. C₂₁H₁₇FeN₅O₆ (491.05): C, 51.35; H, 3.49; N, 14.26 %; Anal. Found: C, 51.43; H, 3.56; N, 14.23%.

1-Ferrocenylmethyl-1*H*-1,2,3-triazol-4-ylmethyl terephthalate (15) Yellow powder. Yield: 2.033g (90%). M. p.: 222.6 °C (DSC). FT-IR (KBr): $\nu = 3155$ m, 2955 w, 1715 vs, 1626 m, 1383 m, 1335 m, 1265 vs, 1106 vs, 1044 m, 801 m, 718 m, 490 s cm⁻¹. **¹H NMR** (400 MHz, CDCl₃): δ 8.04 (s, 4H), 7.59 (s, 2H), 5.43 (s, 4H), 5.30 (s, 4H), 4.01 (s, 4H), 4.23 (s, 4H), 4.18 (s, 10H). **¹³C NMR** (101 MHz, CDCl₃): δ 166.47 (OOC), 143.27 (NCCH), 134.62 (NCCH), 130.59, 124.24 (C₆H₄), 81.47, 70.05, 69.88 (C₅H₄), 69.81 (C₅H₅), 59.45 (C₅H₄CH₂), 51.07 (OCH₂). Calcd. C₃₆H₃₂Fe₂N₆O₄ (724.12): C, 59.69; H, 4.45; N, 11.60 %; Anal. Found: C, 59.62; H, 4.52; N, 11.55%.

1-Ferrocenylmethyl-1*H*-1,2,3-triazol-4-ylmethyl phthalate (16) Yellow powder. Yield: 1.875 g (83%). M. p.: 135.8 °C (DSC). FT-IR (KBr): $\nu = 3094$ m, 2955 w, 1723 vs, 1445 m, 1383 m, 1272 vs, 1120 vs, 1058 s, 940 m, 822 s, 753 m, 490 s cm^{-1} . **^1H NMR** (400 MHz, CDCl_3): δ 7.67 (m, 2H), 7.60 (s, 2H), 7.50 (m, 2H), 5.30 (s, 4H), 5.29 (s, 4H), 4.30 (m, 4H), 4.18 (m, 14H). **^{13}C NMR** (101 MHz, CDCl_3): δ 167.20 (OOC), 142.19 (NCCH), 131.56 (NCCH), 131.28, 129.07, 123.61 (C_6H_4), 80.81, 69.10, 69.01 (C_5H_4), 68.92 (C_5H_5), 58.83 ($\text{C}_5\text{H}_4\text{CH}_2$), 50.13 (OCH_2). Calcd. $\text{C}_{36}\text{H}_{32}\text{Fe}_2\text{N}_6\text{O}_4$ (724.12): C, 59.69; H, 4.45; N, 11.60 %; Anal. Found: C, 59.74; H, 4.48; N, 11.53%.

1-Ferrocenylmethyl-1*H*-1,2,3-triazol-4-ylmethyl isophthalate (17) Yellow powder. Yield: 1.943 g (86%). M. p.: 193.1 °C (DSC). FT-IR (KBr): $\nu = 3087$ m, 2921 w, 1715 vs, 1438 m, 1397 m, 1341 m, 1307 vs, 1231 vs, 1102 s, 1078 s, 961 m, 822 m, 732 s, 482 s cm^{-1} . **^1H NMR** (400 MHz, CDCl_3): δ 8.63 (s, 1H), 8.18 (d, 2H), 7.59 (s, 2H), 7.47 (s, 1H), 5.43 (s, 4H), 5.30 (s, 4H), 4.29 (s, 4H), 4.22 (s, 4H), 4.18 (s, 10H). Calcd. $\text{C}_{36}\text{H}_{32}\text{Fe}_2\text{N}_6\text{O}_4$ (724.12): C, 59.69; H, 4.45; N, 11.60 %; Anal. Found: C, 59.63; H, 4.39; N, 11.68%.

Bis(ferrocenylmethyl-1*H*-1,2,3-triazol-4-ylmethyl) 3-nitrophthalate (18). Dark brown powder. Yield: 1.799 g (75%). M. p.: 226.2 °C (dec, DSC). FT-IR (KBr): $\nu = 3087$ w, 2914 w, 1730 vs, 1612 m, 1536 vs, 1460 m, 1356 s, 1265 vs, 1141 s, 1106 s, 1044 s, 822 m, 711 m, 482 s cm^{-1} . **^1H NMR** (400 MHz, CDCl_3): δ (d, $J = 15.0$ Hz, 2H), 7.69 (s, 1H), 7.63 (d, $J = 19.0$ Hz, 2H), 5.43 (s, 2H), 5.34 (s, 2H), 5.32 (s, 4H), 4.33 (s, 2H), 4.30 (s, 2H), 4.19 (s, 14H). **^{13}C NMR** (101 MHz, CDCl_3): δ 165.90, 164.25 (OOC), 147.12 (CNO_2), 142.49, 142.46 (NCCH), 136.80 (NCCH), 131.51, 131.19, 130.66, 129.33, 124.80 (C_6H_3), 81.71, 70.05, 69.97 (C_5H_4), 69.82 (C_5H_5), 60.63, 60.22 ($\text{C}_5\text{H}_4\text{CH}_2$), 51.07 (OCH_2). Calcd. $\text{C}_{36}\text{H}_{31}\text{Fe}_2\text{N}_7\text{O}_6$ (769.10): C, 56.20; H, 4.06; N, 12.74 %; Anal. Found: C, 56.15; H, 4.02; N, 12.73%.

Bis(ferrocenylmethyl-1*H*-1,2,3-triazolyl-4-ylmethyl) 4-nitrophthalate (19). Dark brown powder. Yield: 1.987 g (80%). M. p.: 237.8 °C (dec, DSC). FT-IR (KBr): $\nu = 3087$ w, 2921 w, 1730 vs, 1605 m, 1529 s, 1356 s, 1272 vs, 1134 s, 1050 s, 822 s, 732 m, 490 s cm^{-1} . **^1H NMR** (400 MHz, CDCl_3): δ 8.56 (s, 1H), 8.34 (d, $J = 8.5$ Hz, 1H), 7.80 (d, $J = 8.5$ Hz, 1H), 7.64 (s, 1H), 7.61 (s, 1H), 5.32 (s, 8H), 4.31 (s, 4H), 4.20 (s, 14H). **^{13}C NMR** (101 MHz, CDCl_3): δ 166.65, 165.57 (OOC), 149.76 (CNO_2), 142.40, 142.40 (NCCH), 138.43 (NCCH), 133.37, 131.12, 127.07, 125.39,

124.69 (C₆H₃), 81.61, 70.07, 69.91 (C₅H₄), 69.84 (C₅H₅), 60.30 (C₅H₄CH₂), 51.11 (OCH₂). Calcd. C₃₆H₃₁Fe₂N₇O₆ (796.10):C, 56.20; H, 4.06; N, 12.74 %; Anal. Found: C, 56.06; H, 4.15; N, 12.70%.

O,O',O''-Tris(ferrocenylmethyl-1*H*-1,2,3-triazolyl-4-ylmethyl) 1,3,5-benzenetricarboxylate (20). Yellow powder. Yield: 2.777 g (85%). M. p.: 184.1 °C (DSC). FT-IR (KBr): $\nu = 3087$ w, 2942 w, 1730 vs, 1612 w, 1452 m, 1321 m, 1231 vs, 1113 s, 1058 s, 1002 s 995 s, 739 s, 497 s cm⁻¹. ¹H NMR (400 MHz, CDCl₃): δ 8.77 (s, 3H), 7.59 (s, 3H), 5.43 (s, 6H), 5.31 (s, 6H), 4.30 (s, 6H), 4.23 (s, 6H), 4.18 (s, 15H). Calcd. C₅₁H₄₅Fe₃N₉O₆ (1047.15):C, 58.48; H, 4.33; N, 12.03 %; Anal. Found: C, 58.42; H, 4.39; N, 12.00%.

O,O',O''-Tris(ferrocenylmethyl-1*H*-1,2,3-triazolyl-4-ylmethyl) 1,2,4-benzenetricarboxylate (21). Yellow powder. Yield: 2.810 g (86%). M. p.: 278.1 °C (dec, DSC). FT-IR (KBr): $\nu = 3087$ w, 2948 w, 1723 vs, 1633 w, 1445 w, 1231 vs, 1113 s, 1044 s, 995 m, 822 m, 760 w, 495 s cm⁻¹. ¹H NMR (400 MHz, CDCl₃) δ 8.32 (s, 1H), 8.12 (d, $J = 8.1$ Hz, 1H), 7.68 (d, $J = 8.0$ Hz, 1H), 7.63–7.56 (m, 3H), 5.42 (s, 2H), 5.33–5.27 (m, 10H), 4.30 (s, 6H), 4.23 (s, 2H), 4.18 (s, 19H). ¹³C NMR (101 MHz, CDCl₃): δ 167.51, 166.93, 165.50 (OOC), 142.99, 142.81, 142.75 (NCCH), 136.73 (NCCH), 133.39, 133.14, 132.36, 131.33, 130.01, 124.60, 124.34 (C₆H₃), 81.68, 81.41, 70.09, 70.02 (C₅H₄), 69.91, 69.82 (C₅H₅), 60.01, 59.93, 59.56 (C₅H₄CH₂), 51.09, 51.06 (OCH₂). Calcd. C₅₁H₄₉Fe₃N₉O₆ (1047.15):C, 58.48; H, 4.33; N, 12.03 %; Anal. Found: C, 58.41; H, 4.39; N, 12.00 %.

2.3. X-ray crystallography

Suitable X-ray quality crystals of **1**, **9**, **13** and **16**·CH₂Cl₂ were grown by slow diffusion of n-pentane into dichloromethane solution of the above compounds in sealed bottles at 0-5 °C. Single crystal X-ray diffraction studies were conducted on a Bruker D8 QUEST diffractionmeter, which equipped with a Photo 100 CMOS detector. The data were collected using graphite monochromated MoK_α radiation. The crystals were kept at 153 K for **1**, **9**, **16**·CH₂Cl₂ and 293 K for **13** during data collection. Their molecular structures were constructed by direct method using SHELXS-2014 and refined by full-matrix least-squares techniques using SHELX-2014/7 [38]. Their crystallographic data and structure refinement parameters are listed in Table 1. Their

selected bond lengths and angles are given in Table S1. Their hydrogen bonds can be found in Table S2.

(Please insert Table 1 here)

Their crystallographic data (excluding structure factors) have been deposited with the Cambridge Crystallographic Data Centre, CCDC, 12 Union Road, Cambridge CB2 1EZ, UK. Copies of the data can be obtained free of charge through the depository numbers CCDC-1956243 (**1**), CCDC-1956257 (**9**), CCDC-1961098 (**13**), CCDC-1961100 (**16**·CH₂Cl₂) (Fax: (+44) 1223-336-033; or E-mail: deposit@ccdc.cam.ac.uk).

2.4. Computational details

For determining iron-iron distances in the molecules of **15-17** and Catocene (for comparison), the DFT method with the Becke's three parameter hybrid functional and Lee Yang Parr's gradient corrected correlation functional (B3LYP) was used to calculate their optimized geometry and ground state electronic structure [39]. The calculations were performed with the GAUSSIAN-09 program [40]. The LanL2DZ basis set and effective core potential were used for iron atoms and the 6-31G basis sets were used for all other atoms [41]. The nature of all stationary points was confirmed by performing a normal-mode analysis.

3. Results and Discussion

3.1. Syntheses and characterization

The new ferrocene-based 1,2,3-triazolyl compounds **1-21** were synthesized using the classic CuAAC method with high yields. The crude products can be purified rapidly by column chromatography on silicone gel. The new compounds are mostly yellow solid and soluble in CH₂Cl₂, CHCl₃, etc, but the solubility of **17** and **20** is very low and their ¹³C NMR spectra were hardly to be measured. The DSC curves of the new **Fc-TAZs 1-21** were shown in Figures S1 and S2, which exhibited that their thermal decomposition peaks are higher than 200 °C (except **10** with 192 °C), indicative of their high thermal stability and further confirmed by their TG curves (Figures S3 and S4). The formation of 1,2,3-triazolyl rings in the new ferrocenes was evidenced by the medium intensity absorptions ranged between 923 and 937 cm⁻¹ and the strong intensity absorptions in the range of 1037–1052 cm⁻¹ (Figures S5–S8). The absorption bands in the FT-IR

spectra of the novel compounds in the regions of 3109–3087, 1113–1097, 827–816, 502–485 cm^{-1} verified the appearance of ferrocenyl groups in the new compounds. The strong bands around 1730 and 1250 cm^{-1} in their FT-IR spectra can be assigned to the stretching vibrations of carbonyl groups. In their ^1H NMR spectra, it is found that chemical shifts of the proton atoms of 1,2,3-triazolyl groups located in the regions of 8.16–8.20 or 7.55–7.65 ppm depending on the substituents and their positions on the phenyl rings. In their ^{13}C NMR spectra, carbon atoms of the ferrocenyl and the carbonyl groups resonated in the ranges of 68–81 and 160–167 ppm, respectively.

The UV/Vis absorption spectra of the ferrocene-functionalized 1,2,3-triazolyl compounds **1–21** in DMSO (Figures S7–S8) showed strong absorption bands between 290 and 300 nm, which can be ascribed to the $\pi\text{-}\pi^*$ transitions of cyclopentadienyl and phenyl groups, and the shoulders between 318 and 330 nm could be assigned to charge transfer bands of the ferrocenyl groups. Meanwhile, the wide and strong absorption bands spanning from 360 nm to 530 nm with peaks around *ca.* 430 nm, are appointed to the $\pi\text{-}\pi^*$ transitions of the ferrocenyl chromophores. The presence of strong electron-withdrawing nitro groups in the phenyl rings weaken absorption bands of the ferrocenyl groups. The usual weak absorptions, due to the d-d transitions of the Fe^{2+} ions peaked in the range of 440–450 nm, are completely covered by the strong $\pi\text{-}\pi^*$ transitions of the ferrocenyl units [42–45].

3.2 Crystal structures

We grew single crystals of **1**, **9**, **13** and **16**· CH_2Cl_2 successfully to confirm the molecular structures of the new compounds. Their crystal structures are shown in Figure 1. Compounds **1**, **9** and **13** crystallize in the monoclinic space group $P2_1/c$ (**1** and **9**) and $P2_1/n$ (**13**), respectively. Compound **16**· CH_2Cl_2 crystallizes in the triclinic space group $P\bar{1}$. The wR2 of **13** (all data) is 0.43, higher than 0.25, due to bad quality of the single crystals of **13**, which have been grown several times and unfortunately no high-quality single crystals were collected. The distances of Cp rings and the sandwiched Fe atoms are in the range of 1.6443(7) Å to 1.6591(5) Å. The dihedral angles between the planar rings in the molecules are of striking difference owing to the appearance of methylene spacers between phenyl, triazolyl and ferrocenyl groups. For examples, the dihedral angles are 63.179(90)° (**1**) and 80.711(56)° (**9**) between the substituted Cp rings and

the 1,2,3-triazolyl rings, 24.795(76)° (**1**) and 59.514(61)° (**9**) between the 1,2,3-triazolyl rings and the phenyl rings. The molecules are linked by weak inter- and intramolecular C–H···N and C–H···O hydrogen bonds into three-dimensional networks, but no classical hydrogen bonds exist in the molecules (Table S2).

(Please insert Figure 1 here)

3.3 Electrochemical behavior

Each catalytic reaction should have at least an electron gain and loss procedure during its catalysis. Therefore, it is necessary to investigate electrochemical behavior of the novel **Fc-TAZs**, including determining their redox reversibility and comparing their oxidation potentials with those of TBF, NBF and Catocene, to estimate their possibility as potential BRCs in solid propellants. Generally, CV is employed to analyze redox properties of ferrocene-based BRC candidates [15-26]. CV curves of the new ferrocenyl compounds in DMSO in the presence of 0.10 M Bu₄NBF₄ as the supporting electrolyte are illustrated in Figure S11 and their numerical information is listed in Table S3. The appearance of only one pair of redox peak for each bis- or trisferrocenyl compound indicated that there is a simultaneous transfer of more electrons in the multinuclear ferrocenyl compounds, due to no considerable electron transport between their ferrocenyl groups. The measured $E_p^{1/2}$, ΔE_p and I_p^a/I_p^c in the ranges of 538-551 mV, 75-105 mV and 1.14-1.43 (except $I_p^a/I_p^c = 1.82$ for **1**), respectively, suggested that more than half of them exhibit reversible Fc/Fc⁺ waves. It is also observed that the oxidation potentials of the new **Fc-TAZs** are higher by *ca* 150 mV than those of TBF, NBF and Catocene, indicative of their higher anti-oxidative ability on comparison with those neutral ferrocenes in DMSO. Effects of the strong electron-withdrawing nitro groups on the redox potentials of the new **Fc-TAZs** are negligible. Moreover, the redox properties of the new compounds may give us useful information in better understanding catalytic activity and the prevalent electron-transfer mechanism of the ferrocene-based BRCs for AP thermal decomposition.

(Please insert Figure 2 here)

3.4 Anti-migratory and anti-volatility studies

Neutral ferrocene derivatives with lower molecular weights such as ferrocene (Fc) and NBF migrate obviously when the composite solid propellants using them as ingredients stored for a long time and thus give rise to a series of problems that affect combustion properties of the

propellants. For dealing with the high-migration problem of the neutral alkyl-substituted ferrocenes, we synthesized a series of ferrocene-based 1,2,3-triazolyl compounds. Anti-migration property of the **Fc-TAZs 1-4, 6, 7, 9-12, 16, 18 and 21** were tested with Fc and Catocene as references under similar conditions. Anti-migration sample preparation details and the measurement procedures are similar to that described previously [16], except the migration temperature was kept at 50 °C to accelerate their migration rates. From the photos shown in Figures S10–S24 it is noticed that both Fc and Catocene migrated considerably even after one week aging, whilst all tested **Fc-TAZs** exhibited no obvious diffusion after four weeks storage. The negligible migration of the new compounds has probably a strong correlation with the non-classic weak hydrogen bonding interactions and van de Waals forces between the propellant components and the novel ferrocenes [22]. These weak interactions are caused by the presence of polar oxygen and nitrogen atoms in the molecules of the tested ferrocene derivatives, AP and

(Please insert Figures 3 and 4 here)

cross-linked HTPB. The migration distances versus storage time are illustrated in Figure 3. It is observed that both Fc and Catocene migrated longer distances (2.5 cm and 1.7 cm, respectively) after four weeks aging. Meanwhile, the tested **Fc-TAZs** moved much slowly after aging over a four-week period (< 0.2 cm), indicating that they show high anti-migration property than Fc and Catocene.

The neutral alkylferrocene-based BRCs show noticeable volatility during fabrication of composite propellants and leads probably to their non-uniform distribution issues in the propellant columns. Additionally, the vaporization and sublimation behavior of the BRCs may give rise to other unanticipated danger [5-9]. Therefore, low-volatility is a necessary property for ferrocene-based BRCs. Increasing polarity of the alkylferrocenes through inserting polar atoms such as O and/or N atoms into their alkyl chains, is a favorable method to improve their anti-volatility property. TG analysis of the new **Fc-TAZs** at 70 °C for 24 h has been carried out to estimate their anti-volatility performance. The results are displayed in Figure 4 and S27. It is noted that Catocene shows *ca.* 4.39% weight-loss after 24h, revealing that Catocene is a relatively high-volatile ferrocene derivative. In contrast, the as-synthesized **Fc-TAZs** displayed negligible weight loss under similar conditions, except **18**, which lost about 1.5% weight after 24 hours, revealing that the new compounds is mostly non-volatile. The consistent-temperature TG analysis confirmed again that functionalization of the alkylferrocenes via insertion of polar O and/or N atoms can tackle their high-migration and high-volatility problems effectively.

3.5 Catalytic performances

In formula of a typical AP-based composite propellant the percentage of the main oxidizer AP is very high and combustion property of AP has intimate correlation with combustion behavior of a classic AP-based propellant. Researchers generally perform TG and DSC studies on thermal decomposition behavior of pure AP and its mixture with a BRC to figure out catalytic effect of the BRC on AP thermal degradation and the results can be used as a pre-estimation for its catalytic activity towards combustion process of a AP-based propellant [46-49].

In these years the traditional AP-based composite propellants are usually modified by addition of other oxidizers such as RDX or HMX to partly substitute AP to lower smoke released by AP and Al powder during propellant combustion and thus increase signal receiving abilities of their IR sensors and reduce detecting possibilities by opposite radars. Thermal degradation performances of RDX and HMX with the as-synthesized ferrocenyl compounds as additives were measured, too.

Concentrations of the new **Fc-TAZs** in the oxidizers were optimized firstly with compounds **1** and **11** as references, based on molecular structural difference between compounds **1-10** and **11-21**. The test results, shown in Figures S28-S33, indicated that the optimal addition amounts in three oxidizers are: 5 wt% in AP and 2 wt% in HMX for both compounds, 4 wt% and 5 wt% in RDX for **1** and **11**, respectively. Therefore, in AP and HMX all compounds were added in 5 wt% and 2 wt%, respectively, but in RDX **1-10** and **11-21** were added in 4 wt% and 5 wt%, respectively.

From Figures 5 and S34, it is found that pure AP started to lose weight at 268 °C and ceased to decomposition at 395 °C. When the **Fc-TAZs** (5 wt%) were mixed with AP, the initial weight-loss temperatures for the mixtures shifted towards left by 3-23 °C to the range of 245–265 °C, indicative of the decomposition of AP in advance in the presence of the new ferrocenes. Meanwhile, the ceased decomposition temperatures of the mixtures, ranging from 337 °C to 353°C, were much lower by 42-58 °C than that of the pure AP. The TG analysis results implied that the **Fc-TAZs** show positive effect on the thermal disintegration of AP.

(Please insert Figure 5 and 6 here)

DSC analysis of the pure AP and its mixtures were additionally performed and their DSC curves were illustrated in Figures 6 and S35. It is noted that the thermal decomposition process of the pure AP has three steps: phase-transition stage, low-temperature stage (LTD) and high-temperature stage (HTD). It is observed that the DSC curves of the mixtures each exhibits three stages, too. The phase-transition temperature of AP (243.6 °C) moved a few degree in the mixtures except its mixture with compound **2** (8.7 °C delay), implying that the additives did not affect the phase transition of AP distinctly. It is observed that most of the mixtures show exothermic peaks in the range of 184-202 °C, which can be assigned to the heat release peaks formed by the catalytic effects of the nano iron oxides on the AP thermal decomposition [46-49]. The nano iron oxides are produced in-situ by the heterogeneous redox interaction of ferrocene derivatives with AP, as observed by other researchers when they studied combustion processes of

AP with ferrocene and other liquid ferrocene derivatives [49-51]. The exothermic peaks appeared around 305 °C and in the range of 341.8-363.3 °C for the mixtures suggested that the LTD stage of AP (peaked at 292.5 °C) shifts right slightly to *ca.* 305 °C and the HTD stage moves dramatically forwards from 406.6 °C by 43.3-64.8 °C. The opposite movement of two stages narrows the temperature span of AP drastically (from 151°C to 75-92 °C), revealing that the AP thermal degradation rate is enhanced with compounds **1-21** as additives and thus demonstrating that the new ferrocenyl compounds exert great effects on the thermal decomposition of AP. The heats released by the mixtures are between -1013 to -1478 J·g⁻¹, with 5 wt.% **6** +AP being the highest, which is almost twice higher than that of AP itself (-746 J·g⁻¹) and higher than that of the mixture of 5 wt.% Catocene +AP (-1303.0 J·g⁻¹). The increment of the released heat of AP verified again that the thermal disintegration of AP is accelerated by addition of the new **Fc-TAZs**.

It is noted that compounds **10**, **15-17**, **18** and **19** are dinuclear ferrocenyl derivatives and **5**, **6**, **20** and **21** are trinuclear ferrocenyl compounds. For studying influence of Fe-Fe distances in these compounds on their catalytic activities towards AP thermal degradation, we calculated Fe-Fe distances in **15-17**. The calculation results exhibited that the Fe-Fe distances in the molecules of **15-17** are 17.38 Å, 18.33 Å and 14.15 Å in gas phase. On comparison, the Fe-Fe distance in Catocene is 6.63 Å in gas phase. The HTD temperature peaks of AP in the mixtures of AP with **15-17** and Catocene are 345.2, 349.3, 345.9 and 342.2 °C, respectively, and the released heats of AP in the mixtures with **15-17** and Catocene are 1189.7, 1361.9, 1271.9 and 1303.0 J·g⁻¹, respectively. From these data we can't give a correlation between the Fe-Fe distance in the binuclear ferrocenyl compounds and their catalytic activities for AP thermal decomposition. In addition, the oxidation potentials of **15-17** in DMSO are 580, 586 and 587 mV, which increase with the increase of the iron-iron distance in their molecules, indicating that with the increase of the Fe-Fe distance the compounds display high anti-oxidation ability, but no imitate correlation between their oxidation potentials and catalytic activities towards AP thermal decomposition was found.

DCS curves of RDX and its mixtures with **1-21**, HMX and its mixtures with **1-21** were shown in Figures S36–S39. Each DSC curve in both Figures S36 and S37 is composed of two or three exothermic peaks, which have never been observed in our previously reported DSC curves of mixtures of RDX and a ferrocene derivative, implying that these new ferrocenyl compounds probably exhibit a different catalytic mechanism during catalyzing RDX thermal degradation [19,20,23-26]. The peak temperature of RDX (231.2 °C) moved right and the released heat of RDX increased (from -827.9 J·g⁻¹ to -862.7 to -1590.0 J·g⁻¹), implying that the as-prepared triazolyl ferrocenyl compounds make no distinct effects on the thermal degradation of RDX. As shown in both Figures S38 and S39, most of the mixtures showed slightly lower peak temperatures than that of pure HMX, suggesting that the new compounds exert positive effect on the thermal decomposition of HMX during combustion. The mixture containing HMX and **1**, **5**, **7**,

8, **11** or **14** releases more heat than that of pure HMX. Taking both peak temperature and released heat into account, compounds **5**, **7** and **11** exhibit considerably positive effect on the thermal degradation of HMX. RDX and HMX are typical nitramines, which are unable to oxidize ferrocenes to form iron oxides at low temperatures, the exothermic peaks are absent on their mixtures' DSC curves up to the main decomposition peaks of RDX and HMX. Therefore, the decomposition peak temperatures of RDX and HMX showed no significant movement to left in the presence of the as-synthesized **Fc-TAZs**, indicating that the new compounds exert unpronounced effects on the thermal decomposition of RDX and HMX on comparison with that of AP.

4. Conclusions

In summary, twenty-one ferrocene-based 1,2,3-triazolyl derivatives were synthesized to tackle the high-migratory problem of the neutral alkylferrocene-based BRCs. The results showed that the newly synthesized ferrocenyl compounds are of high thermal stability and more than half of them show excellent electrochemical reversibility. The tested compounds display much high anti-migration and anti-volatility abilities on comparison with ferrocene and Catocene because of the appearance of polar oxygen and nitrogen atoms in their molecules. TG and DSC results revealed that the new ferrocenyl compounds exhibit high catalytic activity in the thermal degradation of AP during their combustion. Compounds **5**, **7** and **11** as additives can promote thermal decomposition of HMX. It is also concluded that the iron-iron distances and oxidation potentials of the polyferrocenyl compounds have no distinct relationship with their catalytic effect on the thermal decomposition of AP.

Author statement

Wenqian Cheng: Investigation, Methodology, Data curation; **Xiaoling Shi**.: Writing-Original draft preparation. **Yu Zhang**: Software, Visualization; **Yajun Jian**: Writing-Reviewing and Editing.; **Guofang Zhang**: Conceptualization, Supervision.

Declaration of interests

The authors declare that they have no known competing financial interests or personal relationships that could have appeared to influence the work reported in this paper.

Acknowledgements

This work is supported by National Natural Science Foundation of China (21401124, 21602129), Fundamental Research Funds for Central Universities (GK201803027).

References

- [1] J. Prakash Agrawal, High energy materials, WILEY-VCH Verlag GmbH & Co., 2010.
- [2] I. P. S. Kapoor, P. Srivastava, G. Singh, Propellants, Explos., Pyrotech., 34 (2009), 351–356.
- [3] M. Usman, L. Wang, H. J. Yu, F. Haq, M. Haroon, R. Summe Ullah, A. Khan, S. Fahad, A. Nazir, T. Elshaarani, J. Organomet. Chem. 872 (2018), 40–53.
- [4] W. D. Zhou, L. Wang, H. J. Yu, R. B. Tong, Q. Chen, J. H. Wang, X. P. Yang, A. Zain ul, M. Saleem, App. Organometal. Chem., 30 (2016), 796–805.
- [5] D. Saravanakumar, N. Sengottuvelan, V. Narayanan, M. Kandaswamy, T. L. Varghese, J. Appl. Polym. Sci., 119 (2011), 2517–2524.
- [6] K. Subramanian, K. S. Sastri, J. Appl. Polym. Sci., 90 (2003), 2813–2823.
- [7] F. J. Xiao, L. Peng, Y. J. Luo, J. Inorg. Organomet. Polym. Mater., 23 (2013), 315–324.
- [8] R. M. Jagtap, D. R. Kshirsagar, V. H. Khire, M. Maurya, S. K. Pardeshi, Adv. Sci., Eng. Med., 8 (2016), 477–482.
- [9] B. Narasimha Rao, K. Malkappa, N. Kumar, T. Jana, Polymer, 163 (2019), 162–170.
- [10] A. A. Vargeese, K. Muralidharan, V. N. Krishnamurthy, Propellants, Explos., Pyrotech., 40 (2015), 260–266.
- [11] C. Morales-verdejo, C. Maria, J. L. Arroyo, P. Povea, G. Carreño, J. M. Manriquez, J Therm Anal Calorim., 131 (2018), 353–361.
- [12] P. Povea, J. L. Arroyo, G. Carreno, A. Norambuena, P. L. Rios, M. B. Camarada, I. Chavez, J. M. Manriquez, C. Morales-Ver-dejo, Thermochim. Acta, 666 (2018), 181–189.
- [13] J. M. Gao, L. Wang, H. J. Yu, A. G. Xiao, W. B. Ding, Propellants Explos. Protech., 36 (2011), 404–409.
- [14] X. Q. Zhang, Y. Xia, L. Y. Jia, J. J. Chi, W. L. Chang, J. W. Wang, Chin. J. Chem. Propellants & Polym. Mater., 10 (2012), 58–64.

- [15] J. B. Zhuo, H. D. Li, C. X. Lin, L. L. Xie, S. Bai, Y. F. Yuan, *J. Mol. Struct.*, 1067 (2014), 112–119.
- [16] X. S. Gu, S. B. Xie, Q. Chen, S. F. Chen, H. Y. Zhao, Z. X. Bian, *New J. Chem.*, 42 (2018), 13319–13328.
- [17] X. Y. Zhu, X. H. Li, F. J. Han, S. C. Zhang, H. Y. Zhao, Z. X. Bian, *Chin. J. Org. Chem.*, 35 (2015), 922–926.
- [18] C. Y. Wang, J. Z. Li, X. Z. Fan, F. Q. Zhao, W. Q. Zhang, G. F. Zhang, Z. W. Gao, *Eur. J. Inorg. Chem.*, 2015, 1012–1021.
- [19] J. Z. Li, C. Y. Wang, X. N. Gao, F. Q. Zhao, K. Zhao, X. Z. Fan, G. F. Zhang, W. Q. Zhang, Z. W. Gao, *Polyhedron*, 106 (2016), 58–64.
- [20] L. P. Jiang, M. M. Liu, L. Xu, T. R. Dong, J. Z. Li, G. F. Zhang, *Anorg. Allg. Chem.*, 645 (2019), 92–100.
- [21] Z. Abidin, L. Wang, H. J. Yu, M. Saleem, M. Akram, H. Khalid, N. M. Abbasi, R. UllahKhan, *App. Organometal. Chem.*, 31 (2017), e3754.
- [22] M. Usman, L. Wang, H. J. Yu, F. Haq, R. X. Liang, R. S. Ullah, A. Khan, A. Nazir, T. Elshaarani, K. R. Naveed, *Inorg. Chimia Acta*, 495 (2019), 118958.
- [23] X. L. Liu, J. Z. Li, F. Q. Bi, W. Q. Zhang, G. F. Zhang, Z. W. Gao, *Eur. J. Inorg. Chem.*, 2015, 1496–1504.
- [24] X. L. Liu, D. M. Zhao, F. Q. Bi, X. Z. Fan, F. Q. Zhao, G. F. Zhang, W. Q. Zhang, Z. W. Gao, *J. Organometal. Chem.*, 762 (2014), 1–8.
- [25] Z. Y. Cheng, G. F. Zhang, X. Z. Fan, F. Q. Bi, F. Q. Zhao, W. Q. Zhang, Z. W. Gao, *Inorg. Chimia Acta*, 421 (2014), 191–199.
- [26] J. Z. Li, X. N. Gao, E. S. Shao, G. F. Zhang, *Z. Anorg. Allg. Chem.* 643 (2017), 455–463.
- [27] H. C. Kolb, M. G. Finn, K. B. Sharpless, *Angew. Chem., Int. Ed.*, 40 (2001), 2004–2021.
- [28] R. K. Iha, K. L. Wooley, A. M. Nystrom, D. J. Burke, M. J. Kade, C. J. Hawker, *Chem. Rev.*, 109 (2009), 5620–5686.
- [29] F. Amblard, J. H. Cho, R. F. Schinazi, *Chem. Rev.*, 109 (2009), 4207–4220.
- [30] R. B. Sushil, B. Varun, V. Gonela, D. Sashi, T. Arunabha, *Organometallics*, 36 (2017), 2141–2152.
- [31] V. Saravanan, A. Kannan, P. Rajakumar, *New J. Chem.*, 41 (2017), 1714–1722.

- [32] J. Camponovo, J. Ruiz, E. Cloutet, D. Astruc, *Chem. Eur. J.*, 15 (2009), 2990–3002.
- [33] C. Arivazhagan, R. Borthakur, S. Ghosh, *Organometallics*, 34 (2015), 1147–1155.
- [34] H. Y. Zhao, L. Guo, S. F. Chen, Z. X. Bian, *RSC Advances*, 3 (2013), 19929–19932.
- [34] S. Ciampi, P. K. Eggers, G. Le Saux, M. James, J. B. Harper, J. J. Gooding, *Organometallics*, 25 (2009), 2530–2539.
- [36] S. H. Sonawane, M. Anniyappan, J. Athar, S. Banerjee, A. K. Sikder, *RSC Adv.*, 6 (2016), 8495–8502.
- [37] T. Romero, R. A. Orenes, A. Tárraga, P. Molina, *Organometallics*, 32 (2013), 5740–5753.
- [38] G. M. Muller-Buschbaum, *Crystal structure refinement with SHELXL*, *Acta Crystallogr., Sect. C: Struct. Chem.*, 71 (2015), 3–8.
- [39] P. J. Stephens, F. J. Devlin, C. F. Chabalowski, M. J. Frisch, *J. Phys. Chem.*, 98 (1994), 11623–11627.
- [40] M. J. Frisch, G. W. Trucks, H. B. Schlegel, G. E. Scuseria, et al., *Gaussian 09*, Revision C.01, suite of programs for ab initio calculation; Gaussian, Inc, Wallingford, CT, 2010.
- [41] P. J. Hay and W. R. Wadt, *J. Chem. Phys.*, 82 (1985), 270–283.
- [42] T. Farrell, T. Meyer-Friedrichsen, M. Malessa, D. Haase, W. Saak, I. Asselberghs, K. Wostyn, K. Clays, A. Persoons, J. Heck, A. R. Manning, *J. Chem. Soc., Dalton Trans.*, 2001, 29–36.
- [43] B. Bildstein, M. Malaun, H. Kopacka, K.-H. Ongania, K. Wurst, *J. Organomet. Chem.*, 552 (1998), 55–61.
- [44] T. Yamamoto, W. Oi, A. Hashidzume, A. Harada, *Bull. Chem. Soc. Jpn.*, 84 (2011), 918–925.
- [42] W. J. Middleton, E. L. Little, D. D. Coffman, V. A. Engelhardt, *J. Am. Chem. Soc.*, 80 (1958), 2795–2806.
- [45] R. S. Rastogi, G. Singh, B. L. Dubey, C. S. Shukla, *J. Catal.*, 65 (1980), 25–30.
- [46] Q. Yang, S. P. Chen, G. Xie, S. L. Gao, *J. Hazard. Mater.*, 197 (2011), 199–203.
- [47] A. J. Han, J. J. Liao, M. Q. Ye, Y. Li, X. H. Peng, *Chin. J. Chem. Eng.*, 19 (2011), 1047–1051.
- [48] Z. R. Liu, C. M. Yin, Y. H. Kong, F. Q. Zhao, Y. Luo, H. Xiang, *Chin. J. Energ. Mater.*, 8 (2000), 75–79.
- [49] V. P. Sinditskii, A. N. Chernyi, D. A. Marchenkov, *Combust., Expl., Shock Waves (Engl. Transl.)*, 50 (2014), 51–59.

- [50] V. P. Sinditskii, A. N. Chernyi, D. A. Marchenkov, *Combust., Expl., Shock Waves (Engl. Transl.)*, 50 (2014), 158–167.
- [51] B. Z. Jiang, T. P. Wang, *Propellants, Explos., Pyrotech.*, 44 (2019), 513–518.

Scheme, Figure captions and Table title

Scheme 1. Molecular structures of the novel ferrocene-based 1,2,3-triazolyl compounds **1-21**.

Figure 1. Crystal structures of **1, 9, 13** and **16**·CH₂Cl₂. (solvents are omitted for clarity).

Figure 2. Cyclic voltammograms of **11-21** in 0.1 M n-Bu₄PF₆-DMSO with a scanning rate of 0.1 V/s.

Figure 3. Migration distances of the simulated composite propellant samples containing **1-4, 6, 7, 9-12, 16, 18, 21** after 1-4 weeks migration at 50 °C. (**Fc** (ferrocene) and **Cat** (Catocene) were used as references).

Figure 4. TG curves of **11, 13, 16, 18, 21** and **Cat** at 70 °C for 24 h.

Figure 5. TG curves of AP and of the mixtures AP + 5 wt.% **11-21**.

Figure 6. DSC curves of AP and of the mixtures AP + 5 wt.% **11-21**.

Table 1. Summary of the crystallographic data of **1, 9, 13** and **16**·CH₂Cl₂.

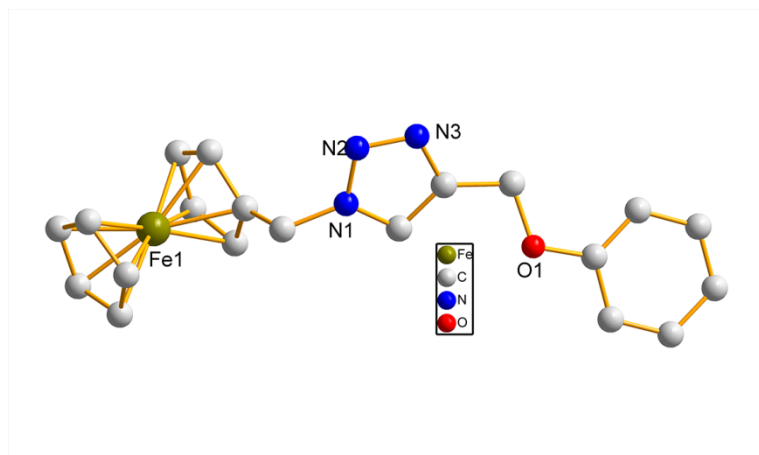
Table 1. Summary of the crystallographic data of **1**, **9**, **13** and **16**·CH₂Cl₂.

Compound	1	9	13	16 ·CH ₂ Cl ₂
formula	C ₂₀ H ₁₉ FeN ₃ O	C ₂₀ H ₁₈ FeN ₄ O ₃	C ₂₁ H ₁₈ FeN ₄ O ₄	C ₃₇ H ₃₄ Cl ₂ Fe ₂ N ₆ O ₄
Fw(g mol ⁻¹)	373.23	418.23	446.24	809.30
T (K)	153(2)	153(2)	293(2)	153(2)
crystal system	monoclinic	Monoclinic	Monoclinic	Triclinic
space group	P2 ₁ /c	P2 ₁ /c	P2 ₁ /n	<i>P</i> $\bar{1}$
a (Å)	5.7232(11)	21.858(4)	5.5889(14)	12.137(3)
b (Å)	23.191(5)	7.8241(14)	31.929(9)	12.766(2)
c (Å)	13.045(3)	10.398(2)	10.698(4)	13.384(3)
α (°)	90	90	90	98.257(7)
β (°)	102.583(7)	94.015(7)	90.976(10)	114.876(7)
γ (°)	90	90	90	104.537(7)
<i>V</i> /Å ³	1689.8(6)	1773.8(6)	1908.7(9)	1746.2(6)
<i>Z</i>	4	4	4	2
<i>D</i> _c (Mg m ⁻³)	1.467	1.566	1.553	1.539
μ (mm ⁻¹)	0.905	0.881	6.666	1.034
Crystal sizes (mm)	0.17×0.13×0.11	0.14×0.12×0.10	0.10×0.08×0.06	0.14×0.12×0.10
reflns collected	11933	20177	12805	20255
Independent reflns	2061	3469	2942	6796
R _{int}	0.0387	0.0385	0.1499	0.0282
GOF on <i>F</i> ²	1.064	1.072	1.799	1.028
R1, wR2 [<i>I</i> ≥ 2σ(<i>I</i>)]	0.0304, 0.0702	0.0295, 0.0734	0.1514, 0.3704	0.0560, 0.1512
R1, wR2 (<i>all data</i>)	0.0372, 0.0725	0.0330, 0.0755	0.2407, 0.4328	0.0606, 0.1560

Highlights

- Ferrocene-based triazolyl compounds (**Fc-TAZs**) were synthesized by click reaction
- **Fc-TAZs** show excellent anti-migratory and anti-volatility properties
- **Fc-TAZs** are highly thermal stable and accelerate thermal degradation of AP

Journal Pre-proofs



Journal Pre-proofs

